Cavitation during Tensile Deformation of Polypropylene

Andrzej Pawlak and Andrzej Galeski*

Centre of Molecular and Macromolecular Studies, Polish Academy of Sciences, Sienkiewicza 112, 90-363 Lodz, Poland

Received July 9, 2007; Revised Manuscript Received February 6, 2008

ABSTRACT: The process of cavitation during tensile deformation of polypropylene was studied. It was shown that in injection-molded polypropylene samples cavities appear in the center of a sample shortly before yielding. With increasing deformation the cavities change their size, number, and orientation from elongated perpendicular to parallel to deformation. The cavitation process is visible also as a rapid increase of volume of deformed material. The cavitation could be suppressed by changing internal morphology of polypropylene by fast cooling. The samples prepared by compression molding followed by quenching, with less perfect crystals, were able to deform by plastic deformation of crystals without cavitation. However, for faster draw rate the cavitation in amorphous phase was preferred again due to stronger response of crystals.

Introduction

The mechanisms of deformation for semicrystalline polymers, among them PP, were subjects of intensive studies in past.[1−12] It is believed that initially tensile deformation includes straining of molecular chains in the interlamellar amorphous phase which is accompanied by lamellae separation, rotation of lamellar stacks, and interlamellar shear. At the yield an intensive chains slip in crystals is observed, leading to fragmentation but not always to disintegration of lamellae. Fragmentation of lamellae proceeds with deformation, and the formation of fibrils is observed for large strains.[13−16] In many papers concerning tensile deformation it was noticed that shortly after yielding some cavities are formed in polymer.[2−4,17,18] The cavitation is not always observed in tensile tests; i.e., the process depends on the material and testing conditions and is never observed in compression of the same material.[1] It was shown in the past that a lamellae fragmentation and cavitation during tensile drawing are often detected simultaneously;[13,19,20] however, it was never proved whether the lamellae fragmentation causes cavitation or vice versa. It seems more probable that the lamellae fragmentation is triggered by cavitation because the lamellae fragmentation causes a release of 3D stress, hence limiting the possibility of cavitation after fragmentation of lamellae.

In the past the cavitation process was treated in the literature as a marginal effect; however, recent studies showed that it may play an important role in the mechanism of plastic deformation.[1,2,9] Usually the cavitation is detected by a small-angle X-ray scattering (SAXS), seen as a rapid increase of scattering intensity. Macroscopically, the intensive voiding is also observed as whitening of a deformed material.

Liu et al.[5] noticed that the whitening of PP during tensile deformation was present in specimens drawn more quickly and at lower temperatures, i.e., when the yield stress was higher. The stress whitening in tensile samples of polyolefins did not occur when the test is conducted under high pressure.[6,7] Yamaguchi and Nitta[8] investigated the intensity of light transmittance while deforming polypropylene. They concluded that the stress whitening is observed beyond the yield point; however, a decrease of transmittance began at a strain of 0.07, i.e., before yielding at strain of 0.15.

Zhang et al.[4] analyzed mechanisms of deformation for polypropylene differently irradiated, tested at selected temperatures. Authors concentrated mostly on polymer microdeformation but evidenced the voids presence in most of samples. They observed that nonirradiated polymer cavitates shortly after the yield, when the temperature was below 60 °C. The SAXS scattering patterns indicate that the cavities change their shape during drawing from initially a peanut-shell-like to lemon-like. Zhang et al.[4] proposed two explanations of shape change: a combination of scattering from primary cavities and a scattering from the voids formed during fibrilation, or primary cavities are elongated to form the voids usually associated with fibrilation.

Some authors observed in drawn polypropylene a presence of crazelike features.[21−25] Crazing was identified long time ago in many glassy polymers, such as polystyrene. Crazes have a shape of planar cracks perpendicular to local strain direction.[26−28] The edges of a crack are bridged by highly oriented polymer fibrils, usually called tufts. They are parallel to the strain direction and are able to carry the load. The thickness of crazes is in the nanometer range, similarly as the thickness of fibrils. Crazes and fibrils can be detected by small-angle X-ray scattering due to nanometer range of their sizes. The characteristic SAXS pattern consists of two components originating from voids and from fibrils, in a form of two perpendicular streaks.[26] One of those streaks, very intense originating from planar crazes, is normal to craze planes while the second, usually less intense, is perpendicular to craze fibrils.[26,27] Crazing is a massive phenomena involved in plastic deformation of glassy polymers.

The features of crazelike structures observed in tensile drawing of PP at temperatures higher than the glass transition temperature are significantly different. First, their thickness is larger, in the range of 1–5 μm. Fibrils inside crazes, 200–650 nm thick,[21] are elongated in the deformation direction; however, a significant fraction of thinner fibrils (20–50 nm) deviate from the principal strain direction.[23] Jang et al.[23] showed that at 23 °C crazing is observed for strain rates higher than 0.11 s^{-2}. Below this limit the deformation mechanism is the shear yielding.[23] Henning et al.[24] by microscopic observations identified positions of intense crazing in deformed spherulitic structure. The conclusion was that crazelike features are visible for α-polypropylene in polar regions of spherulites. Some large-scale, trans-spherulitic crazes were observed by Narisawa et al.[25] passing through equatorial parts of spherulites.

Friedrich[21] and later Kausch[22] reviewed crazing processes in semicrystalline polymers. In their opinion it involves several stages: the initial stage is generally a macroscopically homogeneous deformation involving lamellar tilt and some breakup.

* Corresponding author. E-mail: andgal@bilbo.cbmm.lodz.pl.

10.1021/ma0715122 CCC: $40.75
Published on Web 03/19/2008

At this stage the strain is accommodated almost entirely by the interlamellar amorphous regions.[21] Disruption of lamellae into 10–30 nm size blocks, voiding (with a size of voids 10–50 × 2–6 nm), and formation of fibrils between voids from partly extended tie molecules and crystal blocks characterize the intermediate stage. The third stage, at higher draw ratios, leads to a perfect stretching of the fibrils. The fibrils, spanning the edges of a craze and possessing the strength of about 1−2 orders higher than the yield stress, are able to stabilize the microvoid volume. A lateral coalescence of these voids finally provides a local deformation zone in the shape of a craze. Friedrich limited this description to a low-temperature crazing. The Kausch description[22] differs from the Friedrich envision in that in the first stage the interlamellar separation of lamellae oriented perpendicularly to deformation direction is followed by cavitation and/or crystal plastic deformation and not lamellar fragmentation. Lamellar fragmentation occurs at the intermediate stage.

In an earlier paper by Galeski, Argon, and Cohen[29] the following scenario of voiding under the imposed uniaxial tension was outlined: the packets of lamellae in the 45° fans of spherulites experience resolved shear stress that promote chain slip in the lamellae and shear in interlamellar amorphous regions. Such deformation is accompanied by lattice rotation which generates tensile stresses across the faces in equatorial plates and compressive stresses across the faces in polar fans of spherulites. In addition to these, the overall elongation of spherulites evokes radial pressure on the equatorial planes and additional tensile stresses in the radial direction on the polar fans. Since these accentuated stresses in equatorial lamellae packets have no important shear components either on the interlamellar layers or on the planes of lamellae that promote chain slip, other more damaging types of local plastic deformation are enforced. As is well-known,[30] compression of such composite stacks lamellae and amorphous layers along stiff lamellae gives rise to unstable kinking of the lamellae. This produces periodic undulations in the lamellae ribbons. The accentuated tensile stresses acting across the equatorial disks of a spherulite expand amorphous material within lamellae kinks into pores. Similar and complementary processes are expected to occur in polar fans of spherulites; however, no action is expected from the amorphous phase but, instead, from the lamellae ribbons. In this case the chain fold planes in the lamellae form unstable stacks in tension. Any inhomogeneous lamellae kinks would be filled with amorphous material under transverse pressure, producing no voids. Thus, the end result should be the array of aligned cavities in the equatorial disks of spherulites.

The above-outlined picture of voiding in crystalline polymers above T_g differs significantly from craze formation in glassy amorphous polymers:

1. Formation of aligned voids is triggered by compressive kinking instability along lamellae in equatorial disks of spherulites and not by meniscus instability as in the case of crazes in glassy amorphous polymers. Distances between voids are characteristic for kinking that is dependent on several factors, the most important being the lamellae thickness.[31] The wavelength of kinks in crystalline polymers is usually of order of 200–500 nm. The voids are narrow and long as the width of kinked lamellae.

2. Growth of crazelike entities in equatorial disks of spherulites occurs via plastic deformation of the amorphous material between laterally aligned voids that is transformed further into fibrils. The thickness and length of these fibrils are related to the amount of the amorphous material between voids and that is connected in the first approximation with the lamellae thickness. These fibrils may mimic tufts in crazes of amorphous glassy polymers.

3. Voids in other parts of a spherulite arise at later stages of deformation, and the mechanisms of their formation are different. Since there are no dilatational stresses at 45° fans of spherulites, the interlamellar slip and chain slips in lamellae prevail and no voiding is usually observed.

4. A disruption of lamellae in polar fans of spherulites is required; pores are formed at larger overall strain when the amorphous material becomes unable to fill significantly increased gaps between lamellae fragments. At even further strain the neighboring voids coalesce in planes perpendicular to drawing direction while the amorphous material between these voids is transformed into fibrils. The thickness of those fibrils is related to the thickness of the amorphous layers and depends on the strain at which the voids coalesce and fibrils are formed. These crazelike entities resemble rather thick cracks because fibrils usually break at such high local strain.

The above concept of formation of crazelike objects in crystalline polymers explains the existence of bimodal distribution of fibril thickness and is also supported by recently published AFM studies for initiation of voids in polybutene spherulites and their transformation into crazelike entities with increasing deformation.[32] The crazelike features in polypropylene are seen by electron microscopy; however, in contrast to crazing in glassy amorphous polymers, the fibrils in PP are usually not detectable in SAXS experiments due to a small number of fibrils and their large thickness.

Some SEM observations (e.g., Jang et al.[23]) show fibrils in drawn PP only after etching. However, it is not clear whether they are craze tufts or remnants of initial cross-hatched PP lamellae revealed by etching. The last case seems more reasonable because there are two populations of fibrils; the second one is nearly perpendicular to the first one.

In some other papers (e.g., ref 11) the term "crazing" is misused for the description of microcracks.

Formation and growth of cavities are the main reasons of volume change during tensile drawing. The concept of volume strain, introduced by Bucknall,[33] was recently applied for the studies of semicrystalline polymers.[34–38] The volume strain of cavitating polymers may significantly increase with increasing draw ratio and reach 0.4 for PET[35] and more than 0.15 for PVDF.[36] Recently, Billon et al. observed rapid increase of volume strain for PP, resulting from nucleation of voids in the core of injection-molded polypropylene samples.[39]

It was shown that for most of crystalline polymers including polypropylene and other polyolefins tensile drawing proceeds at a much lower stress than kinematically similar channel die compression.[2,9] Lower stress in tension was always associated with cavitation of the material. Usually a cavitating polymer is characterized by larger and more perfect lamellar crystals, and cavities are formed in amorphous phase before plastic yielding of crystals. If the lamellar crystals are thin and defected, then the critical shear stress for crystallographic slips is resolved at a stress lower than the stress needed for cavitation. Then voiding is not activated. An example of such behavior is low-density polyethylene.[2]

In addition to voiding caused by tensile drawing, some voids may be formed during solidification. Those cavities are located between spherulites and sometimes between radial lamellae inside spherulites.[40,41] The micrometer-sized voids are formed near the completion of crystallization, and their number and size depend on solidification conditions.

The knowledge about influence of such voids on mechanical properties of polymers is not complete yet; however, those cavities are not the objects of this paper.

Table 1. Characteristics of Polypropylenes, According to Producer Data

symbol	polymer	density (g/cm^3)	molecular weight M_w(g/mol)	M_w/M_n	melt flow rate (g/10 min, 230 °C, 2.16 kg)
PPH	PP Novolen 1100H	0.91	4.0×10^5	5.0	1.8
PPN	PP Novolen 1100N	0.91	2.5×10^5	5.0	11.0

Recently, we have studied the cavitation during tensile deformation in high-density polyethylene.[42] The samples were prepared by both injection and compression moldings in order to differentiate their internal structure and perfection of lamellae. It was shown that cavitation in HDPE depends on lamellae thickness and their arrangement. For example, when the crystals were oriented perpendicularly to drawing direction, as in the skin of injection-molded specimen, the cavities were formed readily as early as at 1% of elongation. Cavitation in the core of the same injection-molded HDPE sample was observed at yield (above 10% of elongation). The shape of cavities changes with increasing deformation similarly as it was described by Zhang et al.[4] It was also shown that the same polymer formed by rapid cooling of melt is able to deform without cavitation during tensile drawing.

Polypropylene is a cavitating polymer similar to polyethylene, but the process of cavitation may proceed differently. In this paper we describe the role of molecular weight, crystal thickness, and testing rate on the formation of cavities and their growth during tensile deformation.

Experimental Section

Materials and Methods. Two commercial polypropylenes Novolen by BASF, characterized by different molecular weight (M_w) but with the same M_w/M_n ratio, were selected for our studies. The characteristics of examined polypropylenes, according to the producer data, are presented in Table 1. Samples for mechanical tests were prepared by injection molding. A Battenfeld 30 g injection molding machine was used. The temperature of a barrel was 190 °C, and the temperature of mold was 20 °C. The shape of samples was according to ASTM D638M-93 standard, with 10 mm width, 4.0 mm thickness, and 100 mm gauge length. The mold had a wide entrance, and the speed of injection was low.

A second batch of samples for tensile tests was prepared by compression molding at the temperature of 200 °C, using a hot press. Compression-molded polypropylene Novolen 1100H in the form of 1 mm thick sheets was cooled rapidly in iced water (PPH-W). Dog-bone samples for mechanical tests were then cut from those sheets.

Mechanical tensile properties of PP were studied at room temperature using an Instron model 5582 tensile testing machine. Standard testing rate was of 8.3×10^{-4} s^{-1}; however, some experiments were performed with the rates of 3.3×10^{-3}, 8.3×10^{-3}, and 1.7×10^{-2} s^{-1}. The actual shape of a sample during deformation was recorded by a "Minolta Dimage" digital camera. A mirror was applied for simultaneous recording of the third dimension of a sample, the thickness. The actual cross section was calculated from measured dimensions of the sample. For measurements of the local deformation, black marks were placed on the surface of a sample, at distances of 1 mm, which is similar to the G'Sell approach[35] and to earlier works by Samuels[43] and by us.[44] The local strain was determined as the change of distance between marks, $l - l_0$, divided by the original distance, l_0. The local volume strain was calculated as a change of volume, $\Delta V = V - V_0$, divided by the initial volume, V_0, measured in the most deformed part of a sample. Some of mechanical tests were stopped on a selected level of deformation, and samples after fixing in special frames were studied in the strained state by small-angle X-ray scattering (SAXS).

The small-angle X-ray scattering technique was used for detection of cavities and for determination of long period. A 0.5 m long Kiessig-type camera was equipped with a pinhole collimator and a Kodak imaging plate as a recording medium. The camera was coupled to a Philips PW 1830 X-ray generator (Cu Kα, operating at 50 kV and 35 mA) consisting of a capillary collimator, allowing for resolution of scattering objects up to 40 nm. Exposed imaging plates were read with a PhosphorImager SI system (Molecular Dynamics). The object of studies were both deformed stressed samples and samples after stress relaxation. For the examination of skin the 0.4–0.5 mm thick surface layers were carefully cut out from deformed and relaxed samples by using a razor blade. The intensity of X-ray scattering in semicrystalline polymers is a superposition of contributions from scattering on periodic structure (crystalline−amorphous) and much more intense scattering from voids. If the first component is separated, all registered signal is from voids. According to Guinier approximation,[45,46] if N groups of voids with different sizes exist in material, the intensity of scattering, I, may be described by the equation

$$I = K\sum_{i=1}^{N} v_i \exp(-h^2R_i^2/3) \tag{1}$$

where K is a constant, v_i is the volume of voids in the ith group, R_i is the radius of gyration, and h is the scattering vector. The volume v_i depends on a number of scattering objects, N_i, and, assuming their spherical or ellipsoidal shape, on R_i according to the equation

$$v_i = AN_iR_i^3 \tag{2}$$

where A is constant depending on the geometry of inclusions.

The function ln I vs h^2 was the base for calculation of radii of gyration for each group. Details of the procedure are the same as described by Yamashita et al.[46] Since the function $\ln(I) = f(h^2)$ was not linear for deformed PP, it was divided into 2 or 3 linear parts, each of them representing another population of cavities. The contribution of each group of voids to the total scattering was determined, and radius of gyration was then calculated, beginning with the smallest voids. The voids larger than 40 nm, if present, were not included in calculations because of the limit of SAXS apparatus measurement range.

From the function ln I vs h^2 it is also possible to determine for $h = 0$ the values of $I_{0i} = Kv_i = KAN_iR_i^3$. If the constants K and A are unknown, the absolute numbers of v_i and N_i cannot be determined, but a relative fraction of each group may be easily calculated.

From the preliminary observations we know that the Guinier approach could not be applied for the determination of voids size in the second, perpendicular direction because most of the scattering is inside the SAXS beam stop area. Grubb and Prassad[47] and later Wu[48] and co-workers[49] developed the method of calculation of the second, larger size of cavities or fibrils forming crazes from SAXS results even if the full SAXS pattern is not available. The method is based on analysis of many scattering profiles perpendicular to the direction in the analysis by the Guinier method. The approximated shape of a scattering curve in the center of beam stop is interpolated from perpendicular scattering profiles. The integral breadth Δz of that scattering profile is related to the length of scattering objects according to the equation

$$\frac{(\Delta z)^2\cos(2\Theta)}{\lambda D} = \frac{1}{2l} + \left[\frac{1}{4l^2} + \frac{q^2\sin^2\beta}{4\pi^2}\right]^{1/2} \tag{3}$$

where $q = 4\pi \sin\theta/\lambda$, 2θ is the scattering angle, λ is the wavelength of the X-ray, D is the sample–detector distance, l is the length of voids, and β is the misorientation factor. The length l and misorientation factor β can be obtained by a nonlinear fit of Δz vs q. The same method may be used for voids not inside crazes.

The original method assumes a presence of a single population of scattering elements. If we have some distribution of sizes, then the integral breadth include widening from all scattering elements. In our polypropylene usually we have two fractions of voids of different sizes, as it is known from Guinier's method. Under two

Table 2. Basic Structural Parameters of PP Samples from DSC and SAXS

		DSC		SAXS		
sample	position inside sample	heat of melting [J/g]	crystallinity [%]	long period from Bragg spacing [nm]	long period from correlation function [nm]	crystal thickness[a] [nm]
PPH	skin	91.0	44	12.0	11.9	5.3
	midpoint[b]	102.3	49	12.8	12.9	6.7
	center	103.1	49.5	14.5	14.5	7.2
PPN	skin	92.1	44	12.1	12.0	5.3
	midpoint[b]	99.3	47	14.3	13.0	6.7
	center	97.0	46.5	14.7	13.8	6.8
PPH-W	center	92.5	44.5	11.7	11.8	5.2

[a] Calculated on the basis of long period measured by SAXS and crystallinity measured by DSC. [b] Midpoint: position at the half distance between center and skin.

assumptions—(a) that the Gaussian profile of total scattering peak may be deconvoluted into two Gaussian peaks representing voids populations and (b) that there is a straight relation of those peaks intensities and scattering volume of each group—it is possible to determine the volume fraction of each group from the total integral breadths. We used a standard procedure in Sigma Plot 10 software (by Systat Software Inc.). Because larger cavities dominated in scattering by volume (more than 90% of scattering volume), then the integral breadth was close to the total integral breadth from eq 3. The obtained results, discussed later, give approximated but reasonable values of the length of scattering objects.

The wide-angle X-ray scattering (WAXS) photo camera was used for observations of lamellae orientation. A source of Cu Kα radiation, operating at 50 kV and 35 mA, was used. Two-dimensional scattered images were recorded by a camera equipped with a Kodak imaging plate. The distance between a sample and recording plate was 5 cm. Exposed imaging plates were analyzed with PhosphorImager SI system (Molecular Dynamics).

The degree of crystallinity was determined from the heat of melting by using a DSC 2920 differential scanning calorimeter (TA Instruments). The 8–9 mg samples were heated up from 20 to 200 °C at a rate of 10 K/min. Properties of skin layers were determined for 0.3 mm thick slices cut parallel to the surface.

Samples for microscopic observations were prepared by using a Tesla ultramicrotome equipped with a glass knife. The 20 μm thick slices were examined by polarized light microscopy. Morphology and shape of cavities in cryogenic fractured samples of deformed polypropylene were examine by a JEOL 5500LV scanning electron microscope (SEM).

Results

Injection-Molded Polypropylene. The structure of injection molded samples PPH and PPN was characterized by DSC and SAXS. The basic parameters are collected in Table 2. The crystallinity of all samples was in the range 44–49.5%. There is a tendency—for both PPH and PPN—that it is highest in the center of injection-molded sample, at a similar level at the midpoint (i.e., at the half distance between center and skin) and 3–5% lower at skin layers. Table 2 includes also the results of long period measurements by SAXS. The largest long period in PPN was found in the center, and it decreases with distance from center. The calculations by the correlation function method[50,51] confirm the results of measurements directly from the scattering intensity profiles. The last column of Table 2 presents calculations of crystal thickness by using crystallinity and long period data. For both PPH and PPN the thickest crystals (7.2 and 6.8 nm, respectively) are noticed in the center of injection-molded samples. Crystals in the skin are significantly thinner (5.3 nm).

Figure 1 presents the evolution of morphologies of injection-molded PPH and PPN samples, evaluated from 20 μm thick slices by polarizing optical microscope when moving from the skin to the center. It is seen that the morphology of polypropylenes depends on the position inside sample. A tiny crystalline structure is present in the skin (Figure 1a,d), when moving

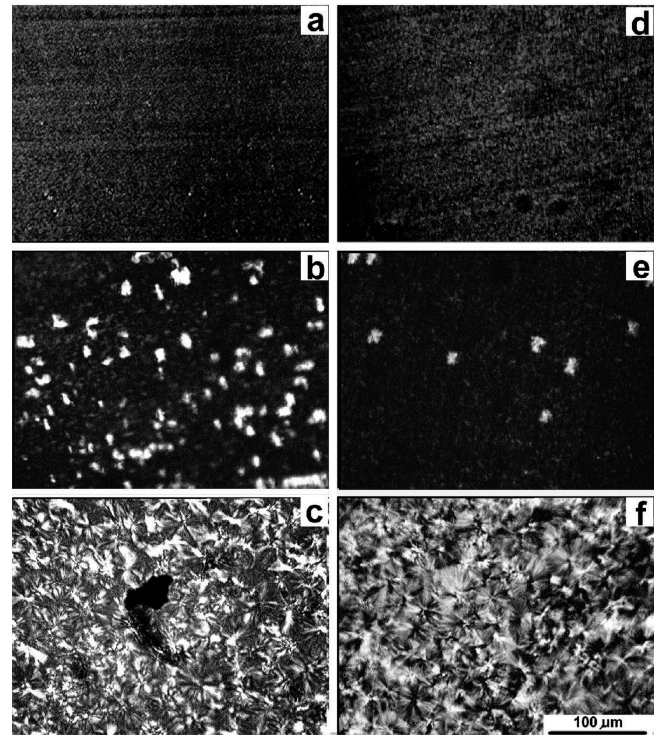

Figure 1. Spherulitic morphology of 20 μm thick polypropylene slices from injected bar observed by polarizing light microscope. PPH: skin (a); middle: 2 mm from skin (b); center (c). PPN: skin (d); middle: 1 mm from skin (e); center (f).

toward the center; isolated spherulites—around 10 μm in size—are visible on the background of small crystalline structures (Figure 1b,e). The number and size of spherulites are larger when closer to the sample center. In the center a volume-filling spherulitic morphology is seen (Figure 1c,f). Individual spherulites have a diameter of 20–30 μm. Near the center of Figure 1c is visible one large black hole, which is a result of cavitation occurring during crystallization. The number of such holes in our samples was limited, and they were usually observed only in the sample centers among volume-filling spherulites.

The crystalline elements in injection-molded samples have very weak preferential orientation. This is concluded from the 2D WAXS diffractograms (not shown here) in which a uniform spatial scattering from crystalline planes for both the core and skin was detected. The presence of α crystallographic phase only was noticed. A similar structure investigation of injection-molded sample was preformed by Fujiyama et al.[52] in which a significant orientation of a skin layer was detected. The difference between the sample preparation in our case was that the injection was through a wide entrance and the speed of injection was low.

Engineering stress—engineering strain curves for injection-molded samples are presented in Figure 2a. Both polymers, PPH

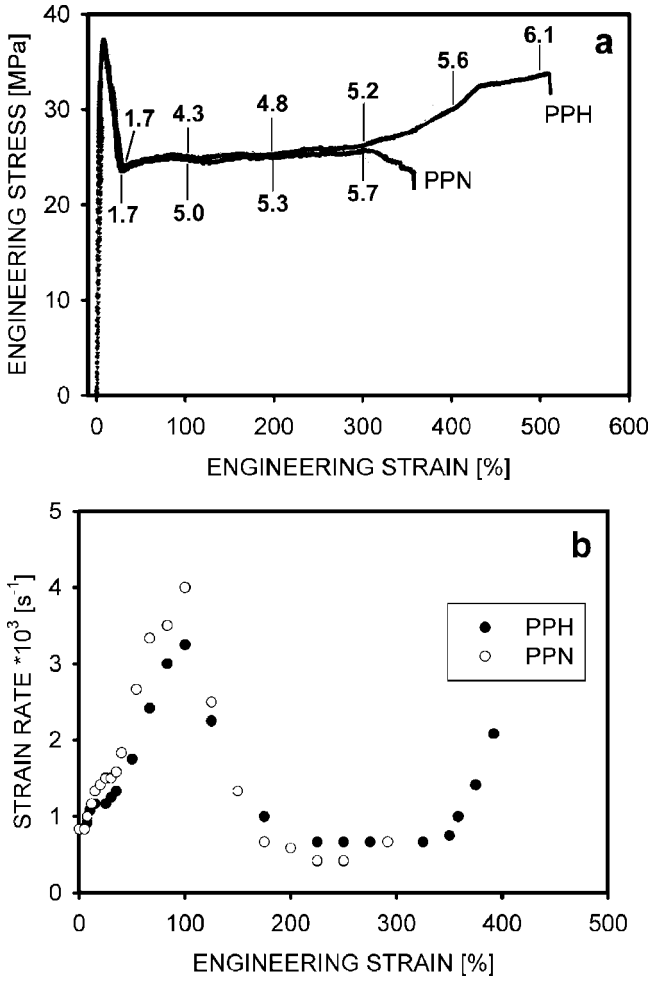

Figure 2. (a) Tensile properties of PPH and PPN. Numbers near curves indicate local strains in most deformed part of each sample. (b) Local strain rate measured for most strained part of sample as a function of engineering strain. Applied engineering strain rate was 8×10^{-4} s^{-1}.

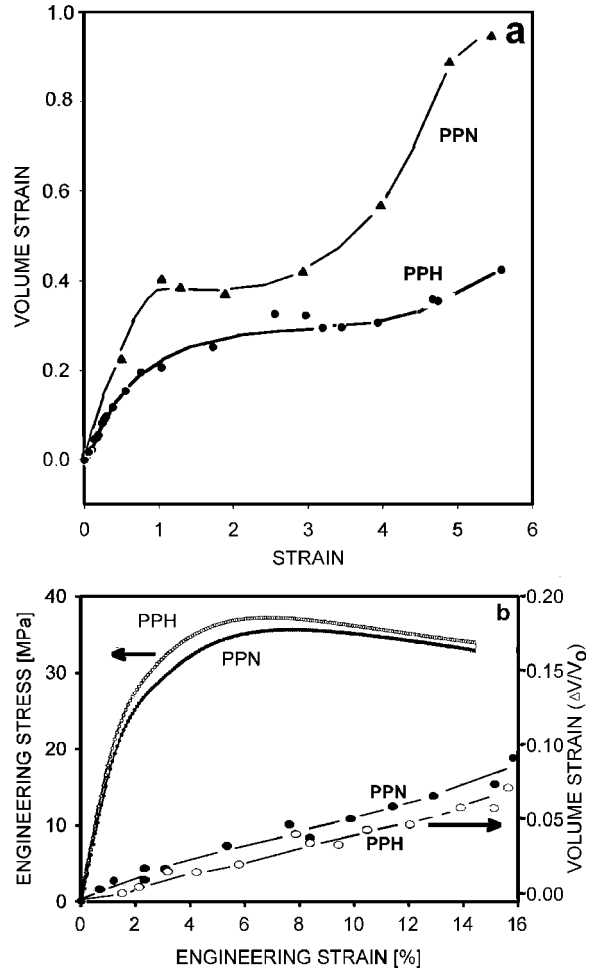

Figure 3. (a) Changes of volume strain with local strain for PPH and PPN. (b) Details of volume strain changes for small deformation. Engineering stress−engineering strain curves are added for comparison.

and PPN, exhibit similar yield properties: the yield stress is at 38 MPa for PPH and 37 MPa for PPN while the yield strain is 7 and 8%, respectively. PPH shows higher elastic modulus 1.62 GPa than lower molecular weight PPN, 1.35 GPa. Beyond the yield point the deformation of both polymers is not homogeneous, and localized necks with local strains much larger than the applied draw ratio were formed. For example, when the engineering strain was 25%, then the maximum local strain was 1.7. The local strains for PPN in a similar range of deformation were close to PPH results. Figure 2a shows that PPH is able to deform even to 500%, which is slightly more than PPN. There is a large increase in local strain for engineering strain between 30 and 100%. The deformation in polypropylene with lower molecular weight is even more localized. The changes in local strain rate as measured for most deformed part of each sample for the engineering strain rate 8×10^{-4} s^{-1} are presented in Figure 2b. Figure 2b illustrates also how nonhomogeneous is the deformation of polypropylenes: a maximum local strain rate was nearly 5 times larger than the engineering strain rate. An interesting observation is that when the neck propagates the local strain rate is below the engineering strain rate.

All deformed samples showed a decrease in translucency. The beginning of strain whitening was observed in PPH and PPN at engineering strain of 5%; it is before yielding. The turbidity was initially increased only in the center of the core of the sample, but the area of whitening quickly propagated to skin, and when the engineering strain reached 7%, only the 0.5 mm thick skin layer was not opaque. When the drawing was stopped at yield (8%) and the sample was relaxed, the permanent whitening was visible in the 1 mm thick core, but in the rest of the sample the translucency approximately came back to its initial level. Apparently, the stress whitening is caused by voids that were formed in the core of a sample. A decrease in whitening after stress relaxation means that some of those voids were able to heal.

Much more intense whitening is observed shortly beyond the yield point, when the neck forms. It spreads over the entire volume of neck with the exception of a skin layer. Outside the neck zone the whitening continuously but less rapidly propagates from the central line to the rest of sample.

The second phenomenon observed during deformation was the change of volume of drawn sample. The measurements of volume strain are presented in Figure 3a while the details for small strains in Figure 3b. Figure 3b also contains engineering stress–strain dependences for illustrating the relations between the volume strain and yielding. It is seen that the volume strain increases from the beginning of drawing; however, initially this increase is not large. PPN shows slightly higher volume strain over the entire range of engineering strain than PPH. Figure 3a shows also that for both polymers there is a rapid increase of volume strain when the engineering strain is in the range from the yield to 1.0. There is a plateau for larger strains; however, when the local strain exceeds 4, the second fast increase of volume strain is seen. The level of plateau and momentary value of volume strain are higher for PPN than for PPH. Since the

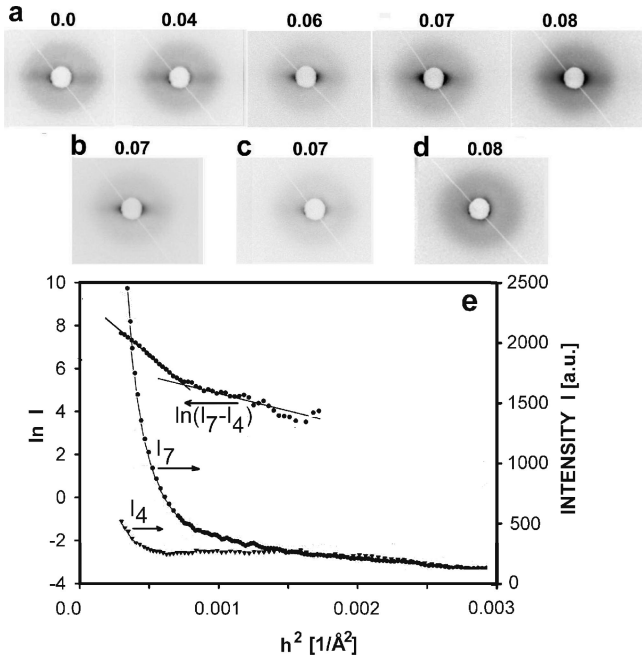

Figure 4. SAXS patterns for PPH samples deformed to different local strains (numbers denote strain). Deformation direction was horizontal. Positions inside the sample: (a) center, (b) middle (2 mm outside the center), (c) middle, after unloading, (d) skin, and (e) horizontal scans of SAXS intensities, primary X-ray beam in the center of sample for 0.04 of local strain (I_4), 0.07 of local strain (I_7), and $\ln(I_7 - I_4)$.

cavitation process is the main factor responsible for the observed increase of volume strain, it means that the scale of cavitation (i.e., number and/or size of cavities) depends on molecular weight and is more intensive in a lower molecular weight polymer.

The injection-molded samples of PPH were the objects of SAXS investigation with the aim of detecting the presence of voids. The results of observation for small deformations, before reaching the yield, are presented in Figure 4. The evolution of scattering pattern in perpendicular illumination is shown in Figure 4a. Up to 0.04 of local strain only X-ray scattering from crystalline structure of polypropylene is visible. However, at the local strain of 0.06 the intensity of scattering rapidly increases in direction of deformation (horizontal in Figure 4). Such rapid increase of scattering is caused by the presence of voids. The contour of the SAXS pattern indicates that the voids are elongated perpendicularly to drawing direction. The intensity of scattering increases with the increase of deformation (0.07). At the same deformation the scattering at the location off the sample center is low (see Figure 4b). It seems that the scattering comes entirely from the core of injection-molded specimen. The cavities located in core of a sample were stable and preserved also when the sample was unloaded. The cavities observed off the center at 0.07 of local strain were not stable, and they mostly healed when unloaded (Figure 4c). Cavitation was not detected in the skin layer before yielding; only scattering from crystals was observed (Figure 4d).

The SAXS scattering intensities are related to the number and volume of scattering objects. Equation 1 can serve for the determination of voids sizes. Since the voids appeared at 0.07 local strain and were not detected for 0.04 local strain (Figure 4a), the 0.04 local strain SAXS pattern was treated as a background and was subtracted from the SAXS pattern for 0.07 local strain.

Figure 4e illustrates this procedure. It shows the profile of intensities along the deformation direction for a sample deformed 0.07 (I_7) and 0.04 (I_4). The third curve, ln ($I_7 - I_4$) represents a natural logarithm of nett signal from voids, after removing of the background intensities I_4, plotted as a function of a scattering vector, h. The last curve is the base for calculations of radii of gyration. The plot according to eq 1 revealed two populations of voids with radii of gyration, R_i, 8 and 18 nm. The number fraction of larger cavities was 82%. Since the scattering from voids in the direction perpendicular to elongation was not observed, all values of R_i were determined in the direction parallel to deformation. It also means that the sizes of cavities in the perpendicular direction were outside the resolution limits of 40 nm. The shape of scattering pattern and values of R_i suggest large dimensions (>40 nm) of voids in the perpendicular to drawing direction. The connected X-ray scattering is at very low angles covered by the beam stop.

The physical origin of two populations of voids is unknown. One of the possibilities is that there is a certain size for stable voids, and the other fraction of voids having smaller size is a kind of embryonic ones. The "embryonic" voids may be stable under stress. Voids smaller than embryonic heal instantly under the action of surface tension, and they are not detected in quasi-steady experiments. The large voids are then preferred.

Ellipsoidal shape of cavities and their preferred orientation transverse to drawing direction is suggested by SAXS pattern. If all ellipsoids representing voids are oriented perpendicular to the deformation direction, their smaller axis is $b = R_i$. The thickness of cavities calculated under assumption of perfect orientation, i.e., $2b = 36$ nm, seems to be unrealistic because it is 5 times thicker than the average amorphous layer.

The other limiting case is random orientation of ellipsoidal cavities: according to equation of $R_i^2 = (a^2 + 2b^2)/5$[53] for the cavities occupying entire thickness of the amorphous layer $2b = 7.2$ nm the longer $2a$ axis of largest population of cavities (with $R_i = 18$ nm) is equal to 80 nm. The SAXS patterns suggest that there is an intermediate state of orientation. It means that the real thickness of cavities is between 7.2 and 36 nm while the longer axis of ellipsoid $2a$ for larger cavities is between 40 (SAXS resolution limit) and 80 nm. For the fraction of smaller cavities for $2b = 7.2$ nm the ellipsoid longer $2a$ axis is only 14.7 nm.

Another way of determination of voids longer axis is by the Grubb and Prasad[47] approach, applied originally for the analysis of crazes length. Using eq 3, a value of 59 nm for larger cavities and 10 nm for smaller cavities are obtained. Those values are in good agreement with previously determined sizes. It is worth to note that the volume fraction of large cavities contributing to scattering is 97%. The low value of misorientation factor in eq 3 confirms that the cavities are approximately oriented perpendicular to the drawing direction.

It means that they are formed in amorphous layers that are also oriented perpendicular to the drawing direction. Amorphous layers having such orientation are located in equatorial parts of spherulites. The location of cavities at early stages of deformation agrees well with the state of knowledge.[17]

The scattering patterns as seen in Figure 4 are from the objects elongated perpendicular to the drawing direction. There is no scattering characteristic for tufts of crazes that are usually observed as thin streaks in the equatorial direction. It means that the scattering objects are not crazes with tufts but there are voids.

Figure 5 presents whitening and X-ray patterns from different parts of PPH sample deformed beyond the yield to the engineering strain of 75% and then unloaded. It is seen that nearly entire gauge length shows whitening, which is especially intensive in the neck region. However, in the skin, even in more deformed regions of neck, the whitening is limited. The SAXS patterns in Figure 5, points "a", "b", and "c", represent scattering from the part of sample deformed to a local strain of 0.3. The

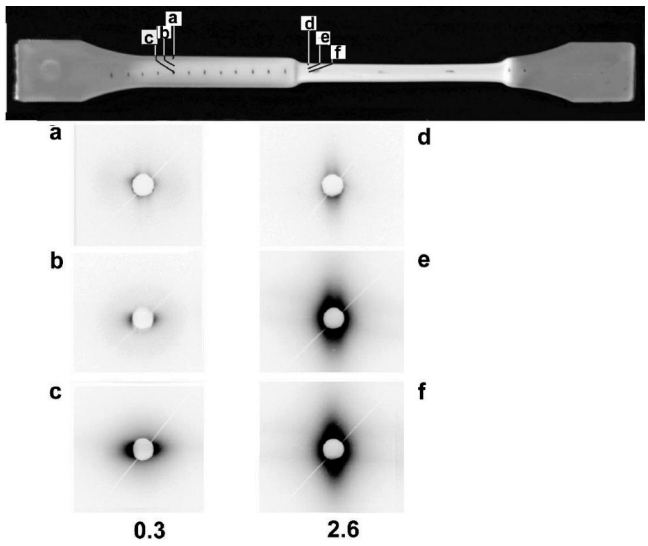

Figure 5. SAXS patterns from different parts of the deformed PPH sample. Numbers indicate local strain.

cavitation is seen only in the center (point "c"), where cavities are elongated perpendicularly to the deformation direction. There is no cavitation in the skin (position "a") and very limited in position "b". The other SAXS paterns in Figure 5, points "d", "e", and "f", represent scattering from the neck area, where local strain was equal to 2.6. It must be noted that the X-ray beam crossed the whole thickness of the sample at points "a−f". However, the SAXS patterns contain mostly information from the core of sample since the skin is free from cavities and does not scatter strongly X-rays. At the large deformation of 2.6 cavities are easily recognized in the center of neck (point "f") and slightly off the center (point "e"). Cavities in the neck are elongated in the deformation direction, and their shape anisotropy is higher in the sample center than off the center. There is an interesting fact that at such high deformation ratio voiding in the skin layer was not detected (in Figure 5, point "d"). In fact, the skin layer is not completely opaque as the rest of the neck area.

From the SAXS patterns in Figure 5 it is evident that in locations with the same local strain the cavities may be formed or not. It seems from Figure 1 and Table 2 that the thickness of crystalline lamellae and local morphology play an important role in cavitation. If lamellae are thick and form spherulitic structure as in the center of injected bar, the cavitation occurs. At positions off the center the lamellae become thinner and the mechanism of deformation changes from cavitational to non-cavitational at the skin. Apparently, in the skin area it is easier to initiate yielding by shear and crystallographic slips than by voiding in the amorphous phase.

The experiment with an injection-molded sample, from which two 1 mm skin layers were removed by machining before the tensile test, shows that the cavitation proceeds similarly as in the corresponding location of a sample with skin layers presented in Figure 5. Cavities near the edge of a sample without skin were observed near yielding. It means that the dominating factor influencing cavitation is a local stress triaxiality between lamellar crystals rather than macro-triaxiality observed previously by Castagnet[54] for samples with large curvature.

The evolution of cavities with increasing deformation can be followed by analysis of SAXS patterns for the core part of injected bar, where the voids were first initiated. The scattering patterns for various deformations of PPH injection-molded samples, recorded after tensile test, are collected in Figure 6a. The scattering from cavities at low deformation (0.1–0.2) is seen in the horizontal section of the patterns. It means that cavities

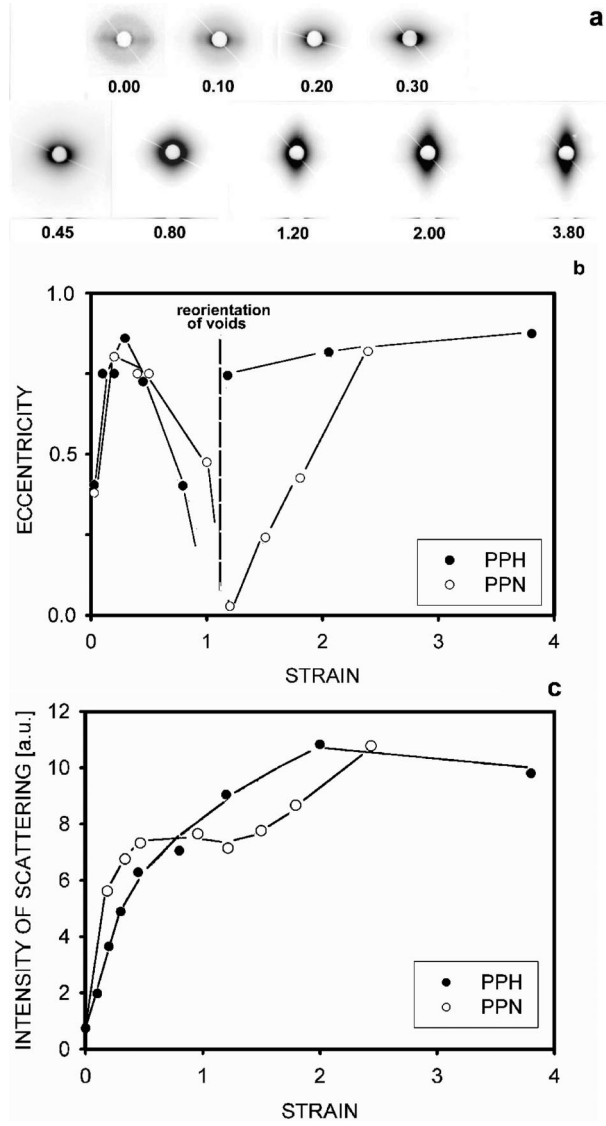

Figure 6. (a) SAXS patterns from central parts of deformed PPH injection-molded samples. Numbers indicate local strains. Deformation direction was horizontal. (b) Eccentricity of scattering pattern as a function of local strain for PPH and PPN injection-molded samples. (c) Dependence of total intensity of SAX scattering on local strain for PPH and PPN injection-molded samples.

are elongated perpendicularly to drawing direction. The shape of voids changes with increasing strain. At the local strain of 0.8 the cavities assumed round shapes (Figure 6a), and for larger deformation (local strain: 1.2–3.8) the cavities are elongated along the deformation direction (maximum scattering is in the direction perpendicular to deformation). These patterns show that at the local strain of around 0.8 we observe a reorientation of cavities. The reorientation of cavities for polypropylene occurs at lower local strain than in similar experiment with HDPE, for which the reorientation begins at the local strain equal to 2.[42]

The of scattering patterns in Figure 6 may be analyzed in a more detailed way by introduction of a new parameter: eccentricity.[55] This parameter was determined by finding points with the same intensity (e.g., half of the maximum) in a pattern and determining lengths of sectors of straight lines between the center of symmetry and points of equal intensity. The lengths of sectors measured in the drawing direction and transverse directions were used for the determination of eccentricity. For elliptical shape the eccentricity parameter is defined by the equation $e = (a^2 - b^2)^{0.5}/a$, where a is the longer and b is the

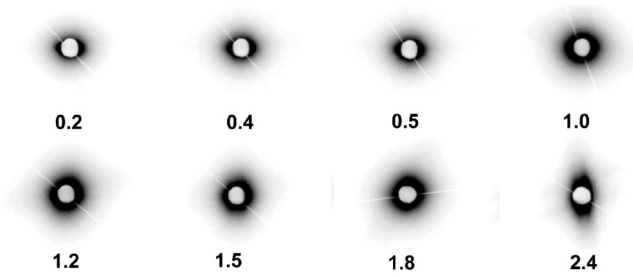

Figure 7. SAXS patterns from the center of PPN samples. Numbers indicate local strain. Deformation direction was horizontal.

shorter semiaxis of the ellipse. The values of eccentricity are presented in Figure 6b for increasing local strains. The curves represent scattering by PPH (SAXS patterns in Figure 6a) and by PPN (SAXS patterns in Figure 7). Initially, the newly formed voids are elongated perpendicular to the drawing direction, and the major axis of SAXS pattern ellipsoid is oriented in the drawing direction. For higher strains the eccentricity increases and for local strains at around 0.2 approaches 0.8–0.85. The eccentricity is reduced to its initial value of 0.0 for local strains of 0.85–1.2. Then for further drawing the shorter (minor) axis becomes larger, and an increase of eccentricity is again observed to a value of 0.87. The second increase of eccentricity factor indicates transformation of the shape of cavities from elongated perpendicular to the drawing direction to elongated along the drawing direction.

The intensity of X-ray scattering from voids increases with deformation (Figure 6c). It is especially visible for local strains in the range 0.2–0.8. The rapid increase of scattering intensity with deformation coincides with a fast increase of the volume strain (Figure 3a), which confirms that the cavitation is a main factor responsible for the increase of volume strain. After reorientation of voids for local strain of 1.2 and more the intensities of SAXS scattering does not seem to increase further. Figure 3 shows also that the volume strain of PPH is preserved for local strains in the range 1.5–4.0. Since the cavities become longer in the deformation direction with increasing local strain, it becomes obvious that the size in the direction perpendicular to deformation is reduced with increasing strain ratio. At local strains higher than 4.0 some cavities long axes are beyond the resolution of SAXS apparatus, and it is probably the reason that the fast increase of volume strain is not accompanied by a significant increase of X-ray scattering from voids.

The second analyzed polymer—PPN—also cavitates during deformation. X-ray scattering patterns for core of PPN injected bar, recorded after tensile test, are presented in Figure 7. The intensity of SAXS from PPN sample deformed to the local strain of 0.2 is larger than that for higher molecular weight PPH (see Figure 6c). A total scattering intensity increases with the deformation and for the local strain equal 1.0 is much higher than for strain of 0.5, suggesting formation of new voids besides the growth of existing voids. At low strains cavities in PPN are elongated perpendicularly to deformation direction. The change of orientation occurs for the local strain range of 1.0–1.2, i.e., similarly as for PPH (see also Figure 6b). At local strains larger than 1.2 the cavities are elongated in the deformation direction. However, in the case of PPN the scattering profile is less elongated in the direction of drawing than it was for highly deformed PPH.

The radii of gyration of cavities for PPH and PPN samples deformed in the range of local strains 0.1–1.0 were determined in the same way as for the PPH sample deformed to 0.07, i.e., using eq 1 and subtracting scattering from noncavitated supermolecular structures. The $\ln I = f(h^2)$ function shows two regions, which are attributed to two populations of cavities,

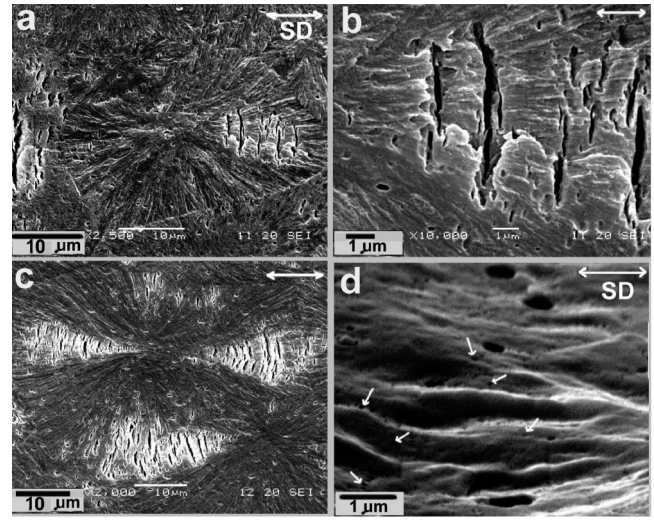

Figure 8. SEM micrographs of morphology of cryogenic fractured deformed PPH samples in the neck region. Strain direction (SD) was horizontal. Local strains: 0.4 (a, b), 0.6 (c), 1.0 (d). White arrows in (d) indicates some of smaller (20–50 nm size) cavities.

independently of the deformation. The number fraction of smaller voids is increasing with increasing local strain and also that fraction is shifted to larger sizes. The number fraction of larger voids decreases with strain, probably because most of them growth and exceed the SAXS detection limit. For example, the cavities in PPH having R_i = 8–9 nm at local strain 0.1 growth and at local strain of 0.3–0.8 are noticed as a group with R_i = 11–13 nm. The fraction of those voids increased from 18% to 65%. Most of voids having at the applied local strain of 0.1 the radius of gyration of 18 nm grew above 40 nm and cannot be detected by our SAXS. Some new smaller cavities are also formed for larger local strains. The two populations ratio is preserved for local strains of 0.3–0.8. However, when compared to Figure 3 and Figure 6c, it is seen that at this range of deformation volume of samples increases rapidly, which means that the total number of cavities increases; i.e., some new small voids are generated while some larger growth and exceed the SAXS detection range. In such a way the number fraction of larger cavities detected is 68–75%, independently of the applied local strain.

The voids length, based on the Grubb—Prasad method, for larger cavities continuously decreases with increasing local strain from 51 nm at local strain of 0.2, through 44 nm at local strain of 0.45 to 19 nm at local strain of 0.8. It is in agreement with the evolution of the shape of SAXS patterns. For the local strain of 0.8 the pattern is nearly circular, and the values for the two directions from the Guinier and Grubb—Prasad methods are 12 and 19 nm. The data of gyration radii for cavities in PPN show that the voids are formed and then transformed similarly as in PPH. The main difference is that the sizes of two populations of cavities in PPN are smaller than in PPH at a similar strain. For example, when the local strain increase from 0.2 to 0.5, the population of voids with R_i = 12 nm disappears, the voids with R_i = 6 nm enlarges to R_i = 9–10 nm, and a new group of voids with R_i = 4 nm is formed. This division is preserved to local strain of 0.8. The radii of gyration for two groups increases to 8 and 11 nm for the local strain of 1.0, when the reorientation process takes place. The length of larger voids determined by the Grubb and Prasad method decreases with deformation from 39 nm at 0.2 local strain to 24 nm at local strain 1.0.

Figures 8 illustrate the alterations of spherulitic structure of PPH during deformation as revealed by scanning electron microscopy. The damage in the form of cracks perpendicular to the drawing direction at polar fans of spherulites is clearly

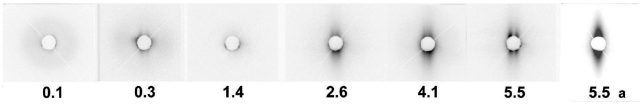

Figure 9. SAXS patterns from the skin of deformed PPH samples. The right-most SAXS pattern corresponds to PPH sample being still under stress. The numbers indicate the local strain in the horizontal direction.

seen at a local strain of 0.4–0.5 (Figure 8a). Some of the cracks are 5 μm long; however, no fibrilar substructure characteristic for crazes is seen (Figure 8b). When the local strain increases to 0.6–0.7, new cracks, slightly smaller in size, appear in the equatorial parts of spherulites (Figure 8c). The cracks in polar locations concentrate more around direction of deformation and open wider. The crazelike substructure, i.e., the presence of fibrils inside cracks, neither in polar nor equatorial zones, is still not detected.

In many parts of spherulites individual cavities are present. The area shown in Figure 8d in higher magnification represents the neck part of the sample in which the local strain was ~1.0. The deformation direction (SD) was horizontal. A few large ellipsoidal cavities oriented in the deformation direction are present. Their long axis is around 0.5 μm long; i.e., they are not detectable by SAXS but are responsible for stress whitening. It is seen that also numerous small cavities are present in the same range of deformation, some of them indicated on the micrograph with white arrows. Those cavities are 20–50 nm in diameter. Smaller cavities are also present, as detected by SAXS, but poorly visible on the micrograph.

The SAXS scattering patterns from the skin part of PPH samples deformed to various degrees are presented in Figure 9. At low and intermediate local strains up to 2.6 the SAXS patterns resemble only the scattering from crystalline elements. At higher deformation of 4.1 the trace of more intensive scattering from voids is seen in the vertical direction, indicating the existence of cavities already elongated in the deformation direction. The more complicated situation is for larger deformation of 5.5, where the scattering pattern with four maxima is formed. Probably, here we have two populations of voids, with long axis tilted at an angle of ~20° with respect to the deformation direction; however, double streaks on SAXS pattern can be also caused by undulated walls of voids or fibrils separated from void walls during unloading. The above considerations are supported by the fact that double streaks in SAXS patterns were never observed for samples being still under stress. Such an SAXS pattern for the PPH sample still being under stress for the draw ratio of 5.5 is illustrated in Figure 9. The number of cavities in skin layer is low as compared to the core of samples. Strong scattering from voids overlaps with relatively weak scattering from crystalline elements.

Since the voids are formed in amorphous layers between crystalline lamellae, the changes of cavity shape should be related to changes in the arrangement of crystalline elements. The alteration of crystalline morphology was determined by WAXS diffraction. The WAXS patterns from central parts of injected PPH samples are shown in Figure 10 for increasing local strain. Deformation direction was horizontal. The concentric rings represents diffraction from the following crystallographic planes: (110), (040), (130), and (111) together with (−131) and (041).[56] In oriented samples the reflections from (110), (040), and (130) tend to concentrate in the direction perpendicular to drawing (the planes for those reflections contain macromolecular chain axes, and they are equatorial in the so-called fiber diffraction pattern); others with the Miller index $l = 1$ and higher form the first and higher layers of a fiber diffraction pattern. Only a very weak initial orientation of

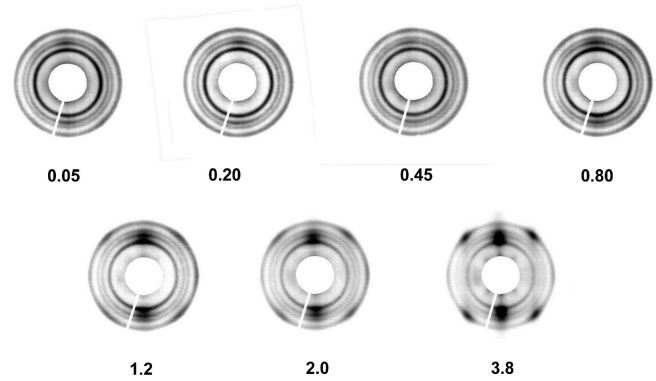

Figure 10. WAXS patterns from the core of PPH samples. Numbers indicate local strain. Deformation direction was horizontal.

crystals in the core of nondeformed PPH is seen that resulted from shear during injection molding. Also, a weak orientation of lamellae stacks perpendicular to the drawing direction was detected by SAXS as presented earlier in Figure 6.

For higher strains the signals from (040) and (110) planes are more and more concentrated at equatorial positions in the fiber diffraction pattern. It suggests that a rotation of crystals either by crystallographic slip or by rotation of lamellae takes place. Which scenario is correct, it cannot be judged at this stage because the SAXS scattering from crystalline lamellae is entirely overlapped with scattering from cavities. The intense rotation of crystals is accompanied by a drastic change of shape of cavities.

The supposition that some fragmentation of lamellae occurs may be verified by analysis of half-width of diffraction peaks using the Scherrer method. The dependence of mean crystal size in the direction perpendicular to (*hkl*) planes, L_{hkl}, on the half-width of diffraction peak is described by the equation $L_{hkl} = 0.9\lambda/(\beta \cos \theta)$, where λ is the wavelength, β the half-width of diffraction peak, and θ the Bragg angle.[57]

The widths of (040) and (130) peaks in PPH were constant for the range of local strains 0–3.5, and the corresponding dimensions of undisturbed crystals were 15.7 and 14.6 nm. The half-width of peak representing scattering from (110) plane increased with deformation. The values of L_{110} were 18.6 nm at the beginning, 17.0 nm at local strain of 0.45, 15.7 nm at local strain of 1.4, and 10.7 nm at local strain of 3.5. The decrease of L_{110} is a result of crystallographic slips (110)[001] along the chain direction, generation of large number of dislocations, and finally lamellae fragmentation. The crystallographic slips (110)[001] along the chain direction was previously found as the main active deformation mechanism for polypropylene.[58] Outer rings of scattering patterns in Figure 10 represent mixed scattering from three planes (111), (041), and (−131), difficult to separate. At the local strain of 1.2 the four-point pattern of the outer ring, representing two populations of differently oriented lamellae, emerges. WAXS scattering from highly deformed samples also shows some presence of the smectic phase, visible on photographs as a diffused black halo between equatorial parts of crystalline rings at angular positions corresponding to reflections from (111), (041), and (−131) planes.

The 2D WAXS patterns recorded from 0.5 mm thick skin layers of PPH are presented in Figure 11. Injection and deformation directions are horizontal. It can be noticed that the crystals are not preferentially oriented, and for the first time the preferred orientation of crystals is noticed for local strain of 1.0. The evolution of crystalline structure in the skin is similar as it was observed in the sample core (Figure 10). The main difference is that the transformations are observed in the core

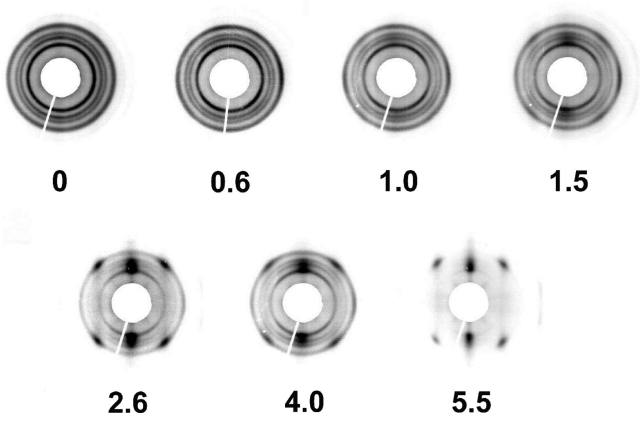

Figure 11. WAXS patterns from the skin of PPH samples. Numbers indicate local strain.

at lower strains, possibly due to higher crystallinity and thicker crystals in the sample core.

Comparison of SAXS (Figures 5−7 and 9) and WAXS results (Figures 10 and 11) leads to the conclusion that shape of cavities formed in the amorphous phase[59–61] depends on the arrangement of crystalline elements. The main transformation of shape, observed at local strains around 0.8, is connected with reorientation of crystals. However, the deformation of lamellae structure may be also realized without cavitation. The example of this is the deformation in the skin of injection-molded samples, where cavities are observed later and are less numerous.

The orientation of those voids depends strongly on the orientation of surrounding crystals that may be deduced from the comparison of SAXS (Figure 9) and WAXS (Figure 11) patterns for the local strain of 5.5.

Up to this point the discussion about cavitation concentrated mostly on the example of higher molecular weight polypropylene (PPH). Observations of the localization of cavities in PPN injection-molded samples as a function of local deformation show that the rules which govern cavitation process in PPN are very similar to those for PPH. The cavities at the beginning are located only in the core, then they change orientation, and some new cavities are visible also farther from the center. The skin layer is resistant to cavitation at small and intermediate local strains, but some traces of voids are visible at higher strains. The studies of wide-angle X-ray diffraction from crystalline structure of PPN show that the deformation of matrix proceeds similarly as for PPH.

The main difference between cavitation in the two types of polypropylene—PPH and PPN—is the higher number of voids in polypropylene PPN, which is manifested by more intensive X-ray small-angle scattering (Figure 7) and larger volume strain (Figure 3) at the same deformation.

Usually in the deformed polymer a partial recovery of strain is observed after releasing of stresses. The full recovery is possible only if the structural elements (e.g., lamellae) are not destroyed or new stable elements of structure (such as voids) are not formed. These conditions are not fulfilled during the plastic deformation; however, some ability to recover is still present, and as proposed by Strobl[13] the analysis of permanent and recovery components of strain may give additional information about the deformation process. Strobl et al. in their experiment used the video equipment to follow in real time the shrinkage of sample subsequent to the release of lower clamp of tensile testing machine. Samples were strained to various strains before the abrupt unloading. We applied this approach for PPH and PPN injection-molded samples. The tensile test of PP samples was stopped at the engineering strains of 30, 50, or 75%. Observations of the samples length after releasing from

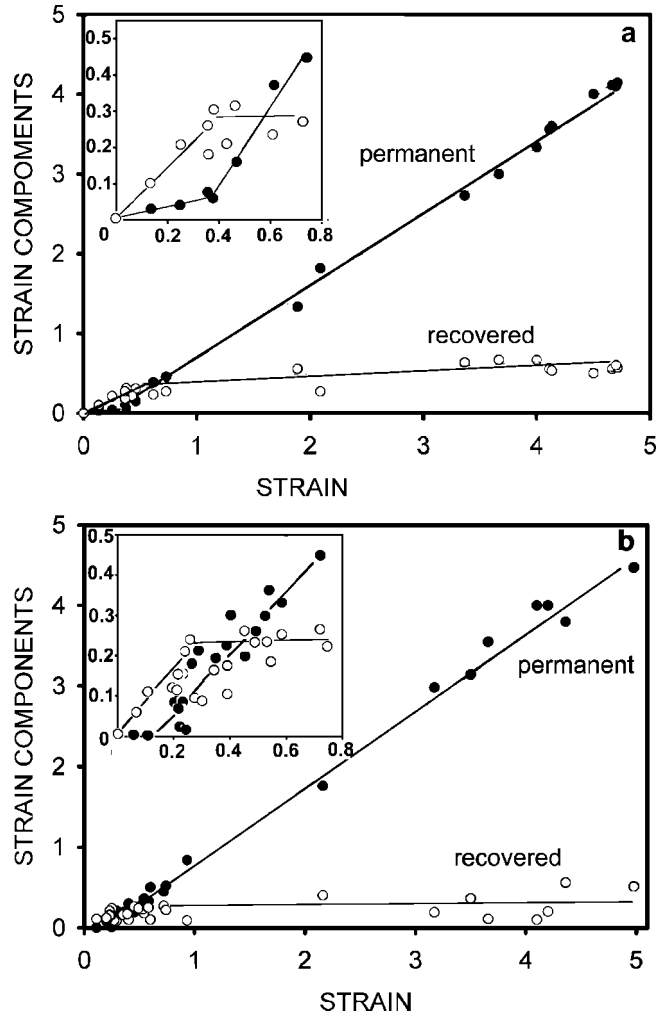

Figure 12. Permanent and recovered components of local strain determined for PPH (a) and PPN (b).

lower grip of the machine showed that it has decreased rapidly during the first minute of observation, but later the decrease was much slower and approximately after 10 min the dimensions of the sample were practically constant. The recovery time seems to be adequate for the determination of relations between permanent and recovered components of strain.

The permanent and recovered strains of PPH and PPN as a function of applied local strain are presented in Figure 12. The permanent strain first appears at yield; however, this component is smaller than the recovered part of total strain up to the applied local strain of 0.5. Above the applied local strain of 0.5 the permanent component increases proportionally to deformation. The increase of permanent strain is observed at lower applied local strain in higher molecular weight PPH. The recovered component of local strain for both PP initially increases linearly with deformation. The values of 0.3 for PPH and 0.25 for PPN are reached for applied local strains of 0.4 and 0.25, respectively. However, for larger strains the increase is small, and for the applied local strain of 5.0 the recovered strain is 0.6 for PPH and 0.35 for PPN. It shows that the recovery is more effective in more entangled, higher molecular weight polypropylene.

The increase of permanent component of local strain is initially mainly due to lamellae slips, as is seen later in PPN, where the amorphous phase may deform easier due to the lower number of entanglements. The significant increase of permanent strain, observed after yield, is a result of intensive cavitation together with further slips in lamellar elements and chain disentanglement in the amorphous phase. This increase is

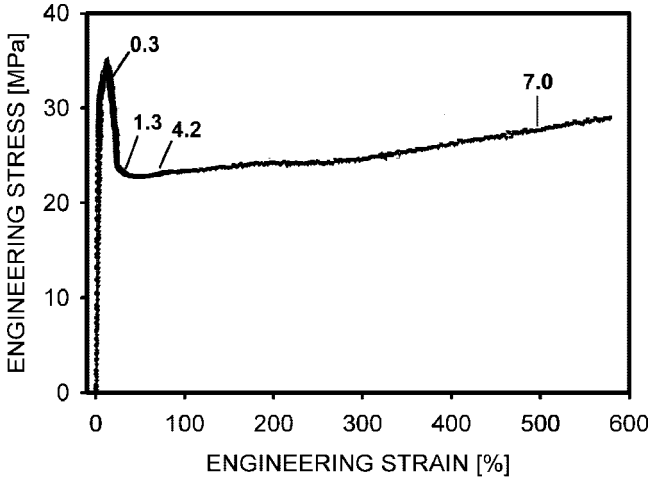

Figure 13. Engineering stress-engineering strain dependence for PPH-W, tested at $v = 8.3 \times 10^{-4}$ s^{-1}. Numbers near the curve represent local strains in the mostly deformed part of sample.

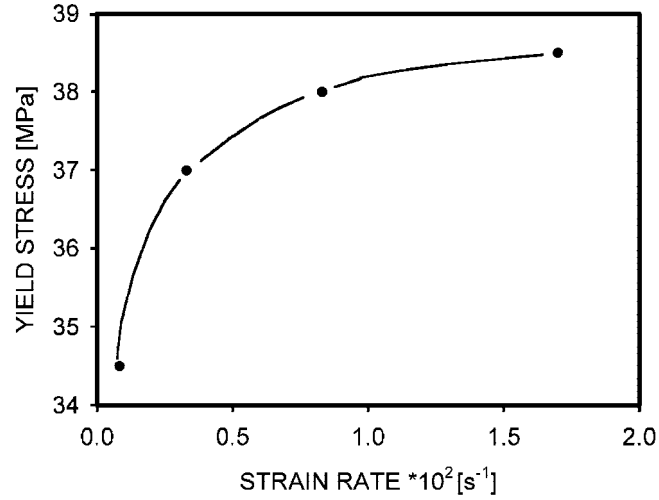

Figure 14. Dependence of yield stress on strain rate for PPH-W.

stronger for lower M_w polypropylene (PPN), where voiding is easier and more effective. A similar conclusion about chain disentanglement was drawn by Strobl.[62] Strobl evidenced, based on the recovery experiments in drawing, that a significant chain untangling takes place.

Compression-Molded Polypropylene. The characteristics of polypropylene sheets prepared by compression molding (PPH-W) are presented in the Table 2. The crystalline structure of PPH-W has the following feature: the lamellae have thickness of 5.2 nm and the crystallinity of 44.5%, which are very close to values for PPH or PPN skin. These observations are supported also by light microscopy examination of 20 μm thick slices from the volume of PPH-W. There are no individual spherulites, and the morphology of the thin slice is very similar to those presented in Figure 1a,d.

Tensile properties of PPH-W tested with a rate of 8.3×10^{-4} s^{-1} are presented in Figure 13. The yielding for this material was at 34.5 MPa, i.e., 2 MPa less than for injection-molded PPH. Yielding was observed at local strain of 0.13, i.e., larger than for PPH (0.08).

The level of yield stress may be modified by changing the testing rate.[63] We also expected that by changing the strain rate it would be possible to influence the cavitation process. However, the experiments done with PPH and PPN injection-molded samples showed that even for very low testing rate (i.e., 8.3×10^{-6} s^{-1}) the cavitation is observed. Our compression-molded samples were more similar to the skin of injection-molded polypropylenes, so it was the chance that the cavitation process can be influenced by varying the strain rate.

Figure 14 illustrates how the yield stress of PPH-W increases with the increase of the deformation rate. The yield stress for the drawing rate of 8.3×10^{-4} s^{-1} was 34.5 MPa, for the rate of 3.3×10^{-3} s^{-1} was 37 MPa, for the deformation rate of 8.3×10^{-3} s^{-1} was 38 MPa, and for 1.7×10^{-2} s^{-1} was 38.5 MPa. Transparency of tested samples decreased with increasing strain rate. The translucency of PPH-W drawn with the rate of 8.3×10^{-3} and 1.7×10^{-2} s^{-1} was much lower than for samples tested with $v = 8.3 \times 10^{-4}$ and 3.3×10^{-3} s^{-1}. The reason for the decrease of transparency was voiding. This conclusion is also supported by the results of volume strain and SAXS measurements.

The results of volume strain measurements are presented in Figure 15. It is seen that the volume strain depends on the local strain and strain rate. There is a significant difference in volume strain of PPH-W at low (8.3×10^{-4} or 3.3×10^{-3} s^{-1}) and high rates (8.3×10^{-3} or 1.7×10^{-2} s^{-1}). In the sample drawn

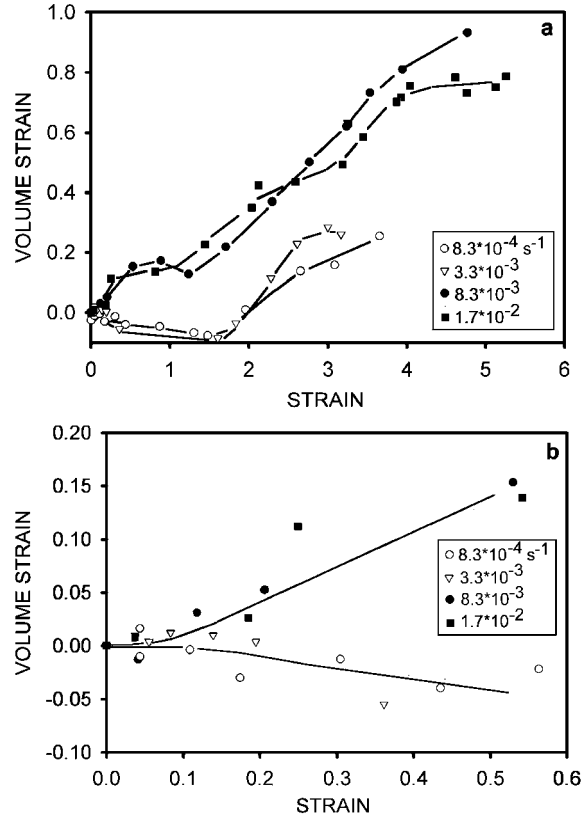

Figure 15. (a) Changes of volume strain for PPH-W as a function of local strain and strain rate. (b) Details for small local strains. The lines show tendencies observed for slow and fast test.

with $v = 8.3 \times 10^{-4}$ s^{-1} a small decrease of volume from 0 to -0.05 is seen when the local strain is increased to 1.5. Such a decrease of volume was previously observed by G'Sell and attributed to the changes in orientation and better packing of the amorphous phase.[34,64] It is interesting that the range of deformations with negative volume strain is much beyond the yield. After reaching the minimum of -0.05 at the local strain of 1.5 an increase of volume strain was observed. At the local strain of 3.6 a 25% increase in volume of a sample is measured. The volume increase is in the same range as it was previously determined for the PPH injection-molded bars (see Figure 3a). Similar changes of volume with deformation were observed also at the strain rate of 3.3×10^{-3} s^{-1}.

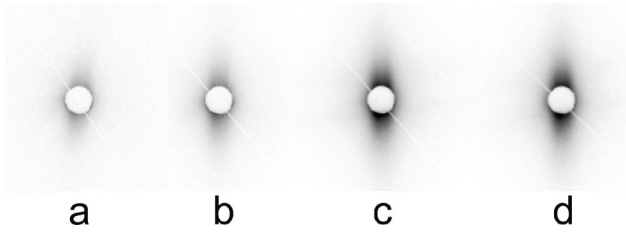

Figure 16. SAXS patterns for samples of PPH-W deformed to engineering strain of 75% with different strain rates: (a) 8.3×10^{-4}, (b) 3.3×10^{-3}, (c) 8.3×10^{-3}, and (d) 1.7×10^{-2} s^{-1}. Deformation direction was horizontal.

The deformation of PPH-W samples drawn with the rates 8.3×10^{-3} and 1.7×10^{-2} s^{-1} proceeded differently (see Figure 15). The volume strain is increasing quickly after the yield. At the local strain of 1.5 the volume strain reaches the value of 0.2. The reason for such increase, as it was confirmed by SAXS results, is the cavitation process. The volume rapidly increases with deformation, and for large local strains of 5–6 it is equal to 0.8–0.9. The comparison of the shapes of curves for fast deformed and slow deformed samples shows that for the volume increase during fast drawing are responsible both cavitation and rearrangement of crystalline structure.

Tensile drawing with different deformation rates were always terminated at the engineering strain of 75%, and the most deformed fragments of samples were investigated by SAXS for detecting voids. The SAXS patterns are collected in Figure 16. On two first images for samples tested with $v = 8.3 \times 10^{-4}$ and 3.3×10^{-3} s^{-1} only the scattering from PP periodic crystalline structure is seen. The samples show at this deformation some orientation of lamellar structure. On the SAXS patterns for samples drawn with faster strain rate (8.3×10^{-3} and 1.7×10^{-2} s^{-1}) an additional scattering from voids appears in the vertical direction, i.e., perpendicular to the deformation direction. The voids at this deformation (local strain around 4.0) are elongated in the deformation direction.

Similarly, as for injection-molded samples the strain recovery of PPH-W was studied. We expected to detect the influence of cavitation on permanent and recovered local strains. The object of studies were samples deformed to 75% of engineering strain with two rates 8.3×10^{-4} and 1.7×10^{-2} s^{-1}. The local strain components of PPH-W are presented in Figure 17. If the sample was tested slowly, the permanent component of strain was nearly zero for local strains below 0.2. The permanent strain for larger deformations increased linearly, but the recovered part of local strain practically stabilized at the level of 0.2. For the strain rate of 1.7×10^{-2} s^{-1} the results were different (Figure 17b). The permanent component was observed earlier around the yield (at local strain of 0.13), which is evidently a result of early cavitation process. The recovered component of local strain stabilized at the level of 0.3, higher than in the case of slowly tested sample.

Conclusions

In experiments we focused on the following points: (a) determination of the relation between molecular weight and cavitation process, (b) showing—similarly as for HDPE—that the occurrence of cavitation depends on the morphology of crystalline structure of semicrystalline polymer, and (c) clarify whether the presence of cavitation depends on strain rate. The injected samples of PPH and PPN deform plastically with necking, and a significant increase of the volume is observed after the yield. The increase of volume is accompanied by intensive whitening of samples. The reason for whitening and volume increase is cavitation initiated in the amorphous phase, which was confirmed by SAXS studies. The volume strain is

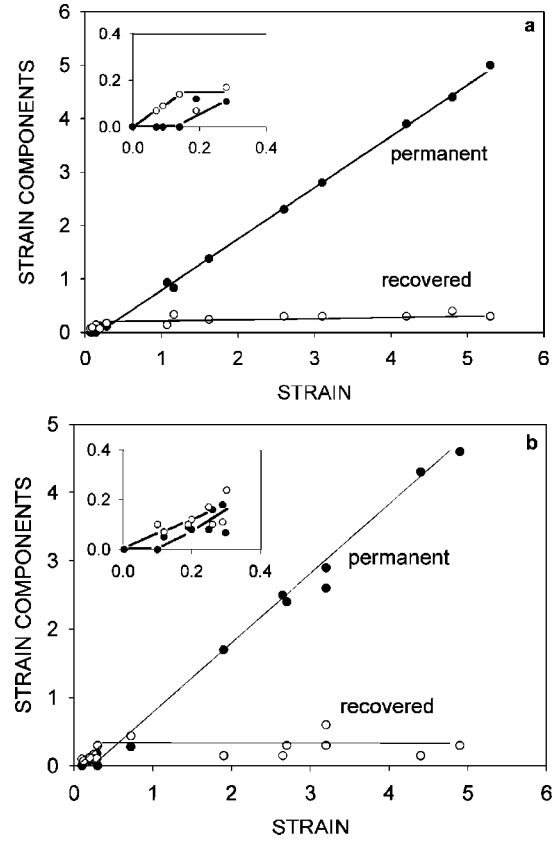

Figure 17. Components of local strain: permanent and recovered, determined for PPH-W deformed with $v = 8.3 \times 10^{-4}$ s^{-1} (a) and $v = 1.7 \times 10^{-2}$ s^{-1} (b).

larger for lower molecular weight PPN polymer, in which the amorphous phase is less entangled. Lower number of entanglements supports easier and more numerous cavitation.

The cavities are formed during tensile drawing in the center of injected samples shortly before yielding. At small local strains, after the yield, a partial healing of small cavities is possible. The zone of cavitation propagates to the rest of sample with increasing deformation.

In the skin of injected samples voids are detected for much higher local strains (larger than 2.6) than in the core of PPH and PPN injection-molded bars. That is because in the skin the crystalline structure is less developed which leads to crystallographic noncavitational mechanism of deformation. The cavitation process occurs when the crystals are enough perfect and strong, i.e., when the stress for plastic deformation of crystals is higher than the stress needed for cavitation of the amorphous phase. At low local strain the cavities are elongated perpendicularly to deformation direction. A typical radius of gyration for voids in PPH is 18 and 12 nm for voids in PPN. If we assume ellipsoidal shape of voids and that their thickness is equal to the amorphous layer thickness (~7 nm), then the lateral size of cavities is around 80 nm in PPH and around 50 nm in PPN. The cavities grow with increasing strain, and also some new voids are formed.

The volume strain does not increase continuously with deformation. There is a plateau in volume strain for applied local strains between 1.0 and 4.0, where the change of internal crystalline structure—orientation and fragmentation of lamellae—leads to a change of voids shape from elongated perpendicular to elongated in the deformation direction. Reorientation process sets in for local strains of 0.8–1.0.

The structure of compression-molded samples is more uniform than the injection-molded bars, so the cavitation occurs

across the whole sample. The presence of cavitation in those samples depends on the strain rate. If the deformation is slow, then the crystalline elements are able to deform plastically before reaching the cavitation threshold of amorphous phase. When the strain rate is higher (i.e., 8.3×10^{-3} or 1.7×10^{-2} s^{-1}), the yield stress, related to crystal strength, is higher (38–38.5 MPa) and cavitation occurs first.

The lack of fibrils bridging the walls of cavities results from the mechanism of their formation within spherulitic structure in crystalline polymers above their T_g as explained in the Introduction.[29] Drawing below T_g may produce crazelike features because inhomogeneous lamellae kinks would not be easily filled with glassy amorphous material under transverse pressure, producing voids and drawing crazy tufts in polar fans of spherulites. The presence of crazes in PP as observed by Jang et al.[23] results probably from a relatively high drawing rate (0.11 s^{-1}) shifting the tough response of PP to the temperature higher than the drawing temperature, whereas in all our experiments the testing rate was kept at least 1 order of magnitude lower (1.7×10^{-2} s^{-1} or lower) than the limit determined by Jang et al.[23] (i.e., 0.11 s^{-1}).

Acknowledgment. The statutory funds of the Centre of Molecular and Macromolecular Studies, Polish Academy of Sciences, Lodz, is acknowledged for providing the financial support for the study. A part of the work was performed under auspices of IUPAC Subcommittee "Structure and Properties of Commercial Polymers".

References and Notes

(1) Galeski, A. *Prog. Polym. Sci.* **2003**, *28*, 1643–1699.
(2) Pawlak, A.; Galeski, A. *Macromolecules* **2005**, *38*, 9688–9697.
(3) Hughes, D. J.; Mahendrasingam, A.; Oatway, W. B.; Heeley, E. L.; Martin, C.; Fuller, W. *Polymer* **1997**, *38*, 6427–6430.
(4) Zhang, X. C.; Butler, M. F.; Cameron, R. E. *Polymer* **2000**, *41*, 3797–3807.
(5) Liu, Y.; Truss, R. W. *J. Polym. Sci., Part B: Polym. Phys.* **1994**, *32*, 2037–2047.
(6) Kapur, S.; Matsushige, S.; Galeski, A.; Baer, E. In *Advances In Research on Strength and Fracture of Materials*; Taplin, D. N. R., Ed.; Pergamon Press: New York, 1978; pp 1079–86.
(7) Pae, K. D.; Chiu, H.-C.; Lee, J. K.; Kim, J.-H. *Polym. Eng. Sci.* **2000**, *40*, 1783–1795.
(8) Yamaguchi, M.; Nitta, K.-H. *Polym. Eng. Sci.* **1999**, *39*, 833–840.
(9) Galeski, A.; Bartczak, Z. *Macromol. Symp.* **2003**, *194*, 47–62.
(10) Peterlin, A.; Balta-Caleja, F. J. *J. Appl. Phys.* **1969**, *40*, 4238–4242.
(11) Dijkstra, P. T. S.; Van Dijk, D. J.; Huetnik, J. *Polym. Eng. Sci.* **2002**, *42*, 152–160.
(12) Lezak, E.; Bartczak, Z.; Galeski, A. *Polymer* **2006**, *47*, 8562–8574.
(13) Hiss, R.; Hobeika, S.; Lynn, C.; Strobl, G. *Macromolecules* **1999**, *32*, 4390–4403.
(14) Butler, M. F.; Donald, A. M.; Ryan, A. J. *Polymer* **1998**, *39*, 39–52.
(15) Wang, K. H.; Chung, I. J.; Jang, M. C.; Keum, J. K.; Song, H. H. *Macromolecules* **2002**, *35*, 5529.
(16) Seguela, R. *e-Polym.* **2007**, 032.
(17) Aboulfaraj, M.; G'Sell, C.; Ulrich, B.; Dahoun, A. *Polymer* **1995**, *36*, 731–742.
(18) Lee, J. K.; Kim, J. H.; Chu, H.-C.; Pae, K. D. *Polym. Eng. Sci.* **2002**, *42*, 2351–2360.
(19) Plummer, C. J. G.; Scaramuzzino, P.; Kausch, H. H.; Phillipoz, J. M. *Polym. Eng. Sci.* **2000**, *40*, 1306–1317.
(20) Plummer, C. J. G.; Beguelin, P.; Grein, C.; Gensler, R.; Dupuits, L.; Gaillard, C.; Stadelmann, P.; Kausch, H. H.; Manson, J. A. E. *Macromol. Symp.* **2004**, *214*, 97–114.
(21) Friedrich, K. In *Advances in Polymer Sciences*; Kausch H. H., Ed.; Springer: Berlin, 1983; Vol. 52/53; pp 225–274.
(22) Kauschp, H.-H.; Gensler, R.; Grein, Ch.; Plummer, C. J. G.; Scaramuzzino, P.*J. Macromol. Sci., Phys.* **1999**, *B38*, 803–815.
(23) Jang, B. Z.; Uhlmann, D. R.; Vander Sande, J. B. *Polym. Eng. Sci.* **1985**, *25*, 98–104.
(24) Henning, S.; Adhikari, R.; Michler, G. H.; Balta Calleja, F. J.; Karger-Kocsis, J. *Macromol. Symp.* **2004**, *214*, 157–171.
(25) Narisawa, I.; Yee, A. F. In *Materials Sciences and Technology. A Comprehensive Treatment*; Thomas, E. L., Ed.; VCH: Weinheim, 1993; Vol. 12, pp 699–766.
(26) Brown, H. R.; Kramer, E. J. *J. Macromol. Sci., Phys.* **1981**, *B19*, 487–522.
(27) Mills, P. J.; Kramer, E. J. *J. Mater. Sci.* **1985**, *20*, 4413–4420.
(28) Zafeiropoulos, N. E.; Davies, R. J.; Schneider, K.; Burghammer, M.; Riekel, Ch.; Stamm, M. *Macromol. Rapid Commun.* **2006**, *27*, 1689–1694.
(29) Galeski, A.; Argon, A. S.; Cohen, R. E. *Macromolecules* **1988**, *21*, 2761–2770.
(30) Argon, A. S. In *Treatise on Materials Science and Technology*; Herman, H., Ed.; Academic Press: New York, 1972; Vol. 1, p 79.
(31) Krumowa, M.; Henning, S.; Michler, G. H. *Philos. Mag.* **2006**, *86*, 1689–1712.
(32) Thomas, C.; Ferreiro, V.; Coulon, G.; Seguela, R. *Polymer* **2007**, *48*, 6041–6048.
(33) Bucknall, C. B. *Toughened Plastics*; Applied Science: London, 1977.
(34) Quatravaux, T.; Elkoun, S.; G'Sell, C.; Cangemi, L.; Meimon, Y. *J. Polym. Sci., Part B: Polym. Phys.* **2002**, *40*, 2516–2522.
(35) G'Sell, C.; Hiver, J.-M.; Dahoun, A. *Int. J. Solids Struct.* **2002**, *39*, 3857–3872.
(36) Castagnet, S.; Girault, S.; Gacougnolle, J. L.; Dang, P. *Polymer* **2000**, *41*, 7523–7530.
(37) Addiego, F.; Dahoun, A.; G'Sell, Ch.; Hivier, J.-M. *Polymer* **2006**, *47*, 4387–4399.
(38) G'Sell, Ch.; Bai, S.-L.; Hiver, J.-M. *Polymer* **2004**, *45*, 5785–5792.
(39) Temimi, N.; Burr, A.; Billon, N. In *Book of Abstracts. Euromech Colloquium 487. Structure Sensitive Mechanics of Polymer Materials: Physical and Mechanical Aspects. Strasbourg 10–13.10.2006*; Remond, Y., Patlazhan, S., Eds.; Strasbourg, 2006; pp 67–68.
(40) Pawlak, A.; Piorkowska, E. *J. Appl. Polym. Sci.* **1999**, *74*, 1380–1385.
(41) Nowacki, R.; Kolasinska, J.; Piorkowska, E. *J. Appl. Polym. Sci.* **2001**, *79*, 2439–2448.
(42) Pawlak, A. *Polymer* **2007**, *48*, 1397–1409.
(43) Samuels, R. J. *J. Polym. Sci., Part C* **1967**, *20*, 253–262.
(44) Kryszewski, M.; Galeski, A.; Pakula, T.; Szylhabel, R. *Polimery (Polish)* **1971**, *16*, 8–11.
(45) Guinier, A. *Ann. Phys.* **1939**, *12*, 161.
(46) Yamashita, T.; Nabeshima, Y. *Polymer* **2000**, *41*, 6067–6079.
(47) Grubb, D. T.; Prasad, K. *Macromolecules* **1992**, *25*, 4575–4582.
(48) Wu, J. *Polymer* **2003**, *44*, 8033–8040.
(49) Wu, J.; Schultz, J. M.; Yeh, F.; Hsiao, B. S.; Chu, B. *Macromolecules* **2000**, *33*, 1765–1777.
(50) Strobl, G. R.; Schneider, M. *J. Polym. Sci., Phys. Ed.* **1980**, *18*, 1343–1359.
(51) Goderis, B.; Reynaers, H.; Koch, M. H. J.; Mathof, V. B. F. *J. Polym. Sci., Part B: Polym. Phys.* **1999**, *37*, 1715–1738.
(52) Fujiyama, M.; Wakino, T.; Kawasaki, Y. *J. Appl. Polym. Sci.* **1988**, *35*, 29–49.
(53) Janosi, A. *Z. Phys B: Condens. Matter* **1986**, *63*, 375–381.
(54) Castagnet, S. *Mater. Sci. Eng., A* **2007**, *448*, 56–66.
(55) *McGraw Hill Encyclopedia of Sciences and Technology*; Lapedes, D. N., Ed.; McGraw-Hill: New York, 1970; Vol. 4, p 638.
(56) Machado, G.; Denardin, E. L. G.; Kinast, E. J.; Goncalves, M. C.; De Luca, M. A.; Teixeira, S. R.; Samios, D. *Eur. Polym. J.* **2005**, *41*, 129–138.
(57) Alexander, L. E. *X-Ray Diffraction Methods in Polymer Sciences*; Wiley-Interscience: New York, 1970; p 335.
(58) Pluta, M.; Bartczak, Z.; Galeski, A. *Polymer* **2000**, *41*, 2271–2288.
(59) Li, J. X.; Cheung, W. L. *Polymer* **1998**, *39*, 6935–6940.
(60) Li, J. X.; Cheung, W. L.; Chan, C. M. *Polymer* **1999**, *40*, 2089–2102.
(61) Li, J. X.; Cheung, W. L.; Chan, C. M. *Polymer* **1999**, *40*, 3641–3656.
(62) Al-Hussein, M.; Strobl, G. *Macromolecules* **2002**, *35*, 8515–8520.
(63) Viana, J. C. *Polymer* **2005**, *46*, 11773–11785.
(64) Cangemi, L.; Elkoun, S.; G'Sell, C.; Meimon, Y. *J. Appl. Polym. Sci.* **2004**, *91*, 1784–1791.

MA0715122